

# WASP-4b Transit Observations With GROND<sup>★</sup>

N. Nikolov<sup>1</sup>, Th. Henning<sup>1</sup>, J. Koppenhoefer<sup>2,3</sup>, M. Lendl<sup>4</sup>, G. Maciejewski<sup>5</sup> and J. Greiner<sup>3</sup>

<sup>1</sup> Max-Planck-Institut für Astronomie, Königstuhl 17, 69117 Heidelberg, Germany  
e-mail: nikolov@mpia.de

<sup>2</sup> Universitäts-Sternwarte München, Scheinerstr. 1, 81679 Munich, Germany

<sup>3</sup> Max Planck Institute for Extraterrestrial Physics, Geissenbachstr., 85748 Garching, Germany

<sup>4</sup> Observatoire de Genève, Université de Genève, 51 chemin des Maillettes, 1290 Sauverny, Switzerland

<sup>5</sup> Toruń Centre for Astronomy, Nicolaus Copernicus University, Gagarina 11, PL87100 Toruń, Poland

Preprint online version: January 5, 2018

## ABSTRACT

**Context.** Ground-based simultaneous multiband transit observations allow an accurate system parameters determination and may lead to the detection and characterization of additional bodies via the transit timing variations (TTVs) method.

**Aims.** We aimed to (i) characterize the heavily bloated WASP-4b hot Jupiter and its star by measuring system parameters and the dependence of the planetary radius as a function of four (Sloan  $g'$ ,  $r'$ ,  $i'$ ,  $z'$ ) wavelengths and (ii) search for TTVs.

**Methods.** We recorded 987 images during three complete transits with the GROND instrument, mounted on the MPG/ESO-2.2m telescope at La Silla Observatory. Assuming a quadratic law for the stellar limb darkening we derive system parameters by fitting a composite transit light curve over all bandpasses simultaneously. To compute uncertainties of the fitted parameters, we employ the Bootstrap Monte Carlo Method.

**Results.** The three central transit times are measured with precision down to 6 s. We find a planetary radius  $R_p = 1.413 \pm 0.020 R_{\text{Jup}}$ , an orbital inclination  $i = 88.^\circ 57 \pm 0.45^\circ$  and calculate a new ephemeris, a period  $P = 1.33823144 \pm 0.00000032$  days and a reference transit epoch  $T_0 = 2454697.798311 \pm 0.000046$  (BJD). Analysis of the new transit mid-times in combination with previous measurements shows no sign of a TTV signal greater than 20 s. We perform simplified numerical simulations to place upper-mass limits of a hypothetical perturber in the WASP-4b system.

**Key words.** transiting planets

## 1. Introduction

More than 100 extrasolar planets have been detected to pass in front of the disk of its parent stars since the first transit observations reported nearly twelve years ago (Charbonneau et al. 2000; Henry et al. 2000; Mazeh et al. 2000). These close-in planets orbit their host stars with periods typically smaller than  $\sim 10$  days, probably formed at greater orbital distances and later migrated inward governed by processes which are still under debate. The discovery of each transiting extrasolar planet is of great interest for planetary science as these objects provide a unique access to an accurate determination of radii (down to a few percent) and masses via transit photometry and radial velocity measurements of the host star (Henry et al. 2000; Charbonneau et al. 2000). Moreover they allow one to plot thermal maps of the planetary surface via infrared spectra (Richardson et al. 2007; Grillmair et al. 2007, Knutson et al 2007), determine the planetary temperature profiles and permit studies of the stellar spin-orbit alignment (Queloz et al. 2000, Triaud et al. 2010, Winn et al. 2011, Johnson et al. 2011). All of these form a set of astrophysically precious parameters, which are critical for constraining the formation and evolution of these interesting objects. Furthermore, the time intervals between successive transits are strictly constant if the system consists of a planet moving on a circular orbit around the parent star. If a third body is present in the system, it would perturb the transiting planet causing the time

interval between successive transits to vary. The resulting transit timing variations (TTVs) allow the determination of the orbital period and mass of the perturber down to sub-Earth masses (Miralda-Escudé 2002, Holman & Murray 2005, Holman et al. 2010, Lissauer et al. 2011).

The transiting planet WASP-4b was discovered by Wilson et al. (2008) within the Wide Angle Search for Planets in the southern hemisphere (WASP-S, Pollacco et al. 2006). The planet is a  $1.12 M_{\text{Jup}}$  hot Jupiter orbiting a G7V star with a period of 1.34 day. WASP-4b was found to have a heavily irradiated atmosphere and inflated radius. Refined planetary orbital and physical parameters, based on transit photometry were presented by Gillon et al. (2009), who used the Very Large Telescope (VLT) to observe one transit, Winn et al. (2009), who measured two transits with the Magellan (Baade) 6.5m telescope at Las Campanas Observatory, Southworth et al. (2009), who observed four transits using the 1.54m Danish Telescope at ESO La Silla Observatory and Sanchis-Ojeda et al. (2011), who observed four transits using the Magellan (Baade) 6.5m telescope. During two of the transits, Sanchis-Ojeda et al. (2011) observed a short-lived, low-amplitude anomaly that the authors interpreted as the occultation of a starspot by the planet. Southworth et al. (2009) also noted similar anomalies in their light curves and the possibility that they were caused by starspot occultations. Sanchis-Ojeda et al. (2011), combined their data set with that of Southworth et al. (2009) and found that each of them is consistent with a single spot and a star that is well-aligned with the orbit. Tracking this starspot, it was possible to measure the rotation period of the host star. A new possible starspot has been re-

<sup>★</sup> Based on observations collected with the Gamma Ray Burst Optical and Near-Infrared Detector (GROND) at the MPG/ESO-2.2m telescope at La Silla Observatory, Chile. Programme 083.A-9010.

cently detected in two closely spaced transits of WASP-4 by the MiNDSTEp collaboration with the Danish Telescope (Mancini 2011, private communication). Furthermore, Beerer et al. (2011) performed space-based secondary eclipse photometry, using the IRAC instrument on the Warm Spitzer Space Telescope, of the planet WASP-4b in the 3.6 and 4.5  $\mu\text{m}$  bands. Their data suggest that WASP-4b’s atmosphere lacks a strong thermal inversion on the day-side of the planet, which is an unexpected result for an highly irradiated atmosphere. Cáceres et al. (2011) analyzed high-cadence near-infrared ground-based photometry, detected the planet’s thermal emission at 2.2  $\mu\text{m}$  and concluded that WASP-4b shows inhomogeneous redistribution of heat from its day- to night-side. Finally, Triaud et al. (2010) investigated the spin-orbit alignment ( $\beta$ ) of the WASP-4 system by measuring the parent star radial velocity during a transit of its planet (Rossiter-McLaughlin effect) and found  $\beta = 4^{+43^\circ}_{-34^\circ}$ , excluding a projected retrograde orbit.

In this paper we present three new transits of WASP-4b observed in August and October 2009 with the GROND instrument (Greiner et al. 2008), attached to the MPG/ESO 2.2m telescope at La Silla Observatory. We recorded each transit in four optical  $g'$ ,  $r'$ ,  $i'$  and  $z'$  (Sloan) channels simultaneously. Using these new data sets we measure the planet orbital and physical parameters and constrain its ephemeris by fitting a new photometric data set over four pass-bands simultaneously. Unlike all previous observational studies related to the WASP-4b exoplanet, that fit data in a single bandpass, we model a transit light curve using the four bandpasses simultaneously. As pointed out by Jha et al. (2000), this approach permits one to break a fundamental degeneracy in the shape of the transit light curve. Each transit light curve can be described primarily by its depth and duration. For a single band observations it is always possible to fit these with a larger planet if the stellar radius is also increased and if the orbital inclination is decreased. The main advantage of the multi-band transit photometry is that it allows the determination of the planet orbital inclination unique, independent of any assumptions about the stellar and planetary radii. Finally, we add the three new mid-transit times and search for TTVs. This paper is organized as follows. In section 2 we present an overview of the three transit observations of WASP-4b and the data reduction. In section 3 we discuss the light curve analysis and the error estimation. Section 4 summarizes the main results.

## 2. Observations and data reduction

Three transits of WASP-4b were observed with the MPG/ESO 2.2-m telescope at La Silla Observatory (Chile) during three runs on UT August 26 and 30 and October 8 2009 (see Fig. 1). Bad weather conditions prevented data collection during the remaining two nights allocated for the project. To monitor the flux of WASP-4, we used the **Gamma Ray Burst Optical and Near-Infrared Detector** (GROND). It is a gamma-ray burst follow-up instrument, which allows simultaneous photometric observations in four optical (Sloan  $g'$ ,  $r'$ ,  $i'$ ,  $z'$ ) and three near-infrared (*JHK*) bandpasses (Greiner et al. 2008). In the optical channels the instrument is equipped with backside illuminated E2V CCDs (2048  $\times$  2048, 13.5  $\mu\text{m}$ ). The field of view for each of the four optical channels is 5.4'  $\times$  5.4' with a pixel scale of 0".158 pixel<sup>-1</sup>.

During each observing run we verified that WASP-4 and a nearby comparison star were located within GROND’s field of view. The comparison star was  $\sim 1.3'$  south-east from our target. For each run we obtained repeated integrations of WASP-4 and the comparison star for  $\sim 3.5$  hr, bracketing the predicted central

transit times. The exposure times were in the range 8–14 s, depending on the weather conditions (i.e. seeing and transparency). During each run we used the fast readout mode ( $\sim 10$  s), achieving a cadence ranging from 18 to 24 s. To minimize systematic effects in the photometry associated with pixel-to-pixel gain variations we kept the telescope pointing stable. However, due to technical issues caused by the guiding camera  $\sim 35\%$  of the total number of images were acquired without guiding, that resulted in  $\sim 10$ -12 pixel drifts per observing run ( $\sim 3.5$  hr).

In the Near-Infrared (NIR) channels we obtained images with integration time of 10 s. Longer exposures are not allowed due to technical constrains in the GROND instrument. It was found during the analysis that the JHK-images were of insufficient signal-to-noise ratio (SNR) to be able to detect the transit and to allow accurate system parameter derivation from the resulting light curves. In addition, the pixel scale in the NIR detectors is 0.6 px<sup>-1</sup>, which resulted in a poorly sampled star psfs (typically 4-5 pixels). As we carried out all observations in the NIR without dithering to increase the cadence and to improve the time sampling and the photometry precision, it is hardly possible to stack groups of NIR images with prior background subtraction. Therefore, we excluded the NIR data in the further analysis.

At the beginning of the observations on UT 2009 August 26 and 30, WASP-4 was setting from an air-mass of 1.02 and 1.05, respectively which increased monotonically to 1.5 and 1.6 at the end of the runs. During the October 8 observations, the air-mass decreased from 1.06 to 1.02 and then increased to 1.15 at the end of the run.

We employed standard IRAF<sup>1</sup> procedures to perform bias and dark current subtraction as well as flat fielding. A median combined bias was computed using 22 zero-second exposure frames and 4 dark frames were used to compute the master dark. As non negligible fraction of the data was obtained without guiding, it was critical to perform the data reduction with flat fields of high quality. A master flatfield was calculated using the following methodology. From a set of 12 dithered twilight flats we selected frames with median pixel counts in the range 10K to 35K which is well-inside the linear regime of the GROND optical detectors. Finally, the reduced (bias- and dark-corrected) flat frames were median combined to produce master flats for each of the  $g'$ ,  $r'$ ,  $i'$  and  $z'$  bands.

Aperture photometry of WASP-4 and the reference star was performed on each calibrated image. To produce the differential light curve of WASP-4, its magnitude was subtracted from that of the comparison star. Fortunately, the later was of similar color and brightness, which reduced the effect of differential color extinction. For example, the instrumental magnitude differences (comparison star minus WASP-4) measured on UT October 8 2009 were  $\Delta g' = 0.587\text{mag}$ ,  $\Delta r' = 0.669\text{mag}$ ,  $\Delta i' = 0.681\text{mag}$ ,  $\Delta z' = 0.687\text{mag}$ . As pointed out by Winn et al. (2009) the comparison star is slightly bluer than WASP-4 ( $\Delta(g' - i') = -0.094\text{mag}$ ).

To improve the light curves quality we experimented with various aperture sizes and sky areas, aiming to minimize the scatter of the out-of-transit (OOT) portions, measured by the magnitude root-mean-square (r.m.s.). Best results were obtained with aperture radii of 16, 20.5 and 17.5 pixels for UT 2009 August 26 and 30 and October 8, respectively.

<sup>1</sup> IRAF is distributed by the National Optical Astronomy Observatories, which are operated by the Association of Universities for Research in Astronomy, Inc., under cooperative agreement with the National Science Foundation.

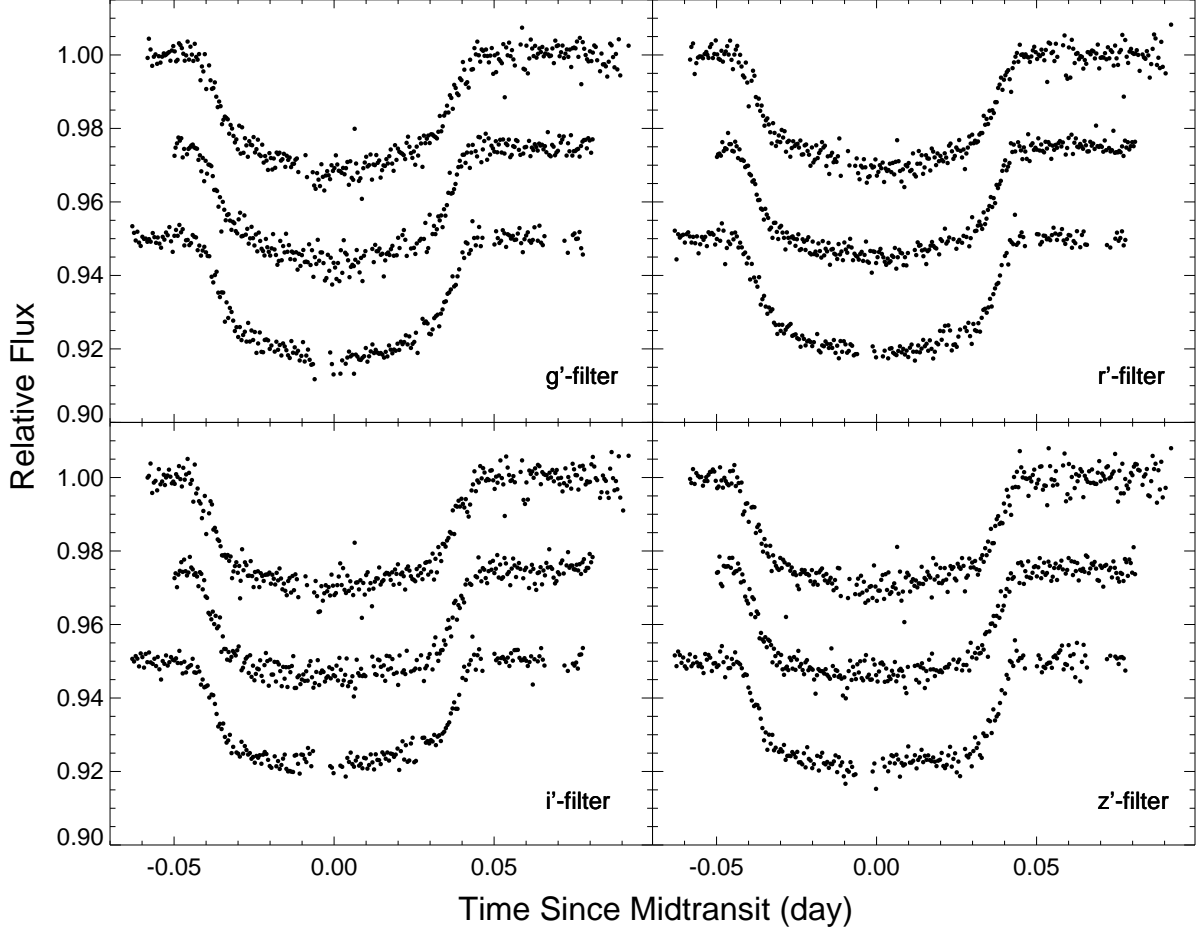


**Fig. 1.** Relative  $g'$ ,  $r'$ ,  $i'$  and  $z'$  -band photometry of WASP-4 obtained with GROND. The transits occurred (for each panel from top to bottom) on UT 2009 August 26, August 30 and October 8. The transit light curves obtained on each successive run are displayed with an offset of 0.025 in relative flux for a better illustration.

The light curves contain smooth trends, most likely due to differential extinction. To improve its quality we decrease this systematic effect using the OOT portions of our light curves. We plot the magnitude vs. air-mass data for each run and channel and fit a linear model of the form:

$$f(z) = a + bz, \quad (1)$$

where ( $a$ ) and ( $b$ ) are constants and ( $z$ ) is the air-mass. Once the coefficients were derived, we applied the correction to both the transit and the OOT data. Performing this correction we notice that the baseline magnitudes of our target and the comparison star show slight, nearly linear correlations with the ( $x, y$ ) center positions of the PSF centroids on each CCD chip. We remove these near-linear trends from WASP-4 and the reference star by modelling the base-line of the light curve with a polynomial that includes a linear dependency on the centroid center positions ( $x$  and  $y$ ) of the stars on the detectors using the function of the form:

$$f(x, y) = 1 + k_x x + k_y y + k_{xy} xy, \quad (2)$$

where ( $k_x$ ), ( $k_y$ ) and ( $k_{xy}$ ) are constants. We then subtracted the fit from the total transit photometry obtained for each channel during the three runs. No other significant trends that were correlated with instrumental parameters were found.

**Table 1.** Light curve scatter difference measured with the standard deviation of the time series prior and after detrending. All quantities in mmag.

run	$g'$	$r'$	$i'$	$z'$
Aug 26	0.503	0.358	0.482	0.339
Aug 30	0.818	0.973	0.633	0.725
Oct 10	0.733	0.614	0.430	0.495

To illustrate the light curve quality improvement we present the scatter decrease after the described detrending procedure (Table 1).

### 3. Light curve analysis

To compute the relative flux of WASP-4 during transit as a function of the projected separation of the planet, we employed the models of Mandel & Agol (2002), which in addition to the orbital period  $P$  and the transit central time  $T_C$  are a function of five parameters, including the planet to star size ratio ( $R_p/R_*$ , where  $R_p$  and  $R_*$  are the absolute values of the planet and star radii), the orbital inclination  $i$ , the normalized semimajor-axis ( $a/R_*$ , where  $a$  is the absolute value of the planet semimajor axis) and two limb darkening coefficients ( $u_1$  and  $u_2$ ). Because the parameters  $a/R_*$ ,  $R_p/R_*$  and  $i$  are degenerate in the transit light curve,

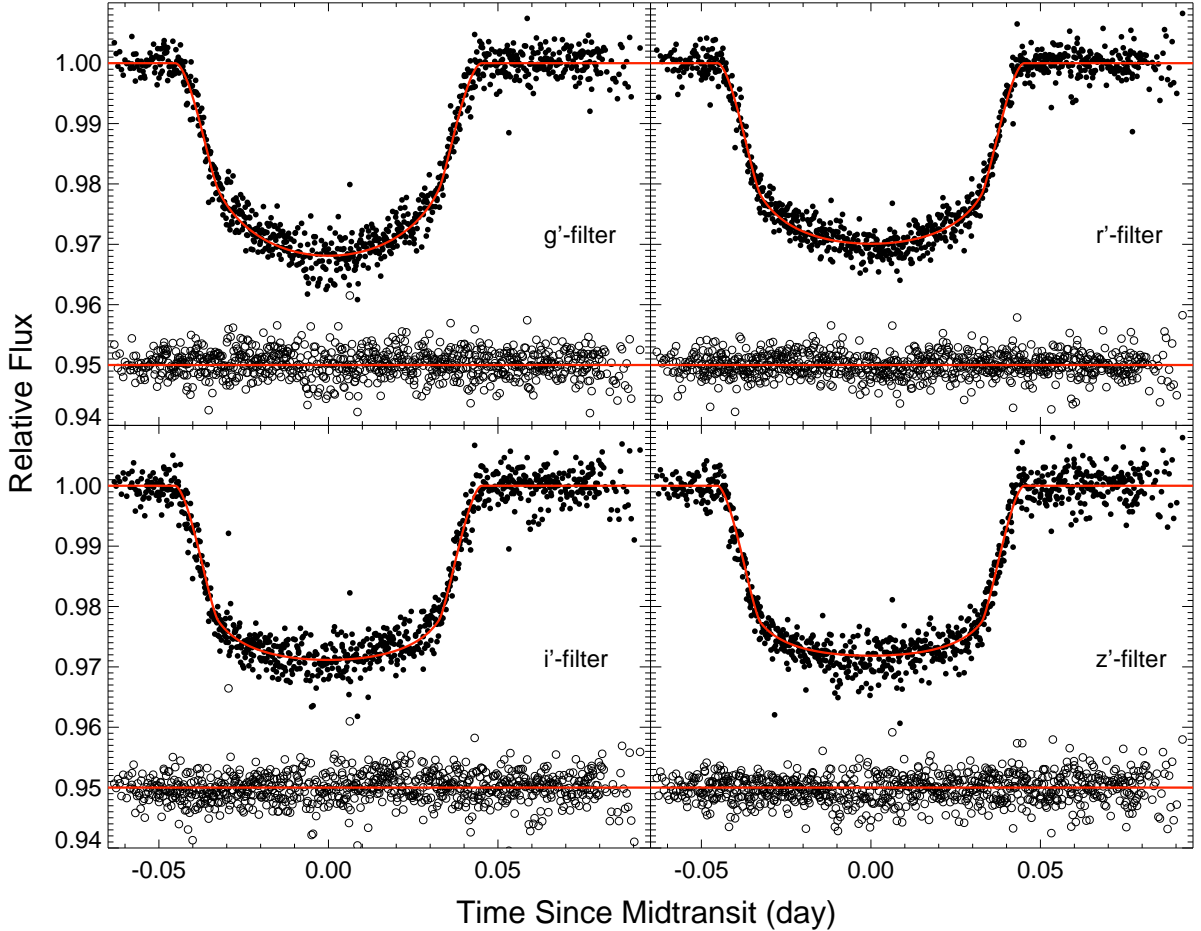


**Fig. 2.** The composite light curves of WASP-4 obtained during three runs on UT 2009 August 26, August 30 and October 8. The best-fit transit models are superimposed with continuous lines and the observed minus modeled residuals are shown centered at flux level 0.95 on each panel along a constant line.

we assume fixed values for  $M_* = 0.92 \pm 0.06 M_\odot$  from Winn et al. (2009) and  $R_* = 0.907_{-0.013}^{+0.014} R_\odot$  from Sanchis-Ojeda et al. (2011) to break this degeneracy. Ideally we would like to fit for all parameters however, only the first three determine the best-fit radius of the star, the radius of the planet, its semimajor axis and inclination relative to the observer.

The values for the two limb darkening coefficients were included in our fitting algorithm to compute the theoretical transit models of Mandel & Agol (2002). We assume the stellar limb darkening law to be quadratic,

$$\frac{I_\mu}{I_1} = 1 - u_1(1 - \mu) - u_2(1 - \mu)^2, \quad (3)$$

where  $I$  is the intensity and  $\mu$  is the cosine of the angle between the line of sight and the normal to the stellar surface. We fixed (initially) the limb darkening coefficients ( $u_1$  and  $u_2$ ) to their theoretical values (see Table 2), which we obtained from the calculated and tabulated ATLAS models (Claret 2004). Specifically, we performed a linear interpolation for WASP-4 stellar parameters  $T_{\text{eff}} = 5500 \pm 100$  K,  $\log g = 4.4813 \pm 0.0080$  cgs,  $[\text{Fe}/\text{H}] = -0.03 \pm 0.09$  and  $v_t = 2.0 \pm 1.0$  km s $^{-1}$ , which we adopted from Winn et al. (2009).

**Table 2.** Theoretical Limb-Darkening Coefficients (Quadratic Law).

LD coefficient	$g'$	$r'$	$i'$	$z'$
wavelength (nm)	455	627	763	893
$u_1$ (linear)	0.623	0.413	0.314	0.248
$u_2$ (quadratic)	0.183	0.290	0.303	0.308

To derive the best fit parameters we constructed a fitting statistic of the form:

$$\chi^2 = \sum_{i=1}^{N_f} \left[ \frac{f_i(\text{observed}) - f_i(\text{predicted})}{\sigma_i} \right]^2, \quad (4)$$

where  $f_i(\text{observed})$  is the flux of the star observed at the  $i$ -th moment (with the median of the OOT point normalized to unity),  $\sigma_i$  controls the weights of the data points and  $f_i(\text{computed})$  is the predicted value for the flux from the theoretical transit light curve. We assume the orbital eccentricity to be zero and minimize the  $\chi^2$  statistic using the downhill simplex routine, as implemented in the IDL AMOEBA function (Press et al. 1992). The minimization method evaluates iteratively the  $\chi^2$  statistic, yet avoiding derivative estimation until the function converges to the global minimum.

In the entire analysis we derive uncertainties for the fitted parameters using the bootstrap Monte Carlo method (Press et al. 1992). It uses the original data sets (from each run and pass-band), with their  $N$  data points to generate synthetic data sets also with the same number of points with replacements. We then fit each data set to derive parameters. The process is repeated until we get an approximately Gaussian distribution for each parameter and take the standard deviation of each distribution as the error of the corresponding fitted parameter.

Ground-based time series data are often prone with time-correlated noise (e.g. “red noise”; see Pont et al. 2006) and therefore the data weights  $\sigma_i$  need a special treatment, i.e. the uncertainties must be calculated accurately in order to obtain reliable estimates of the fitted parameters. It is a common practice to use the calculated Poisson noise, or the observed standard deviation of the out-of-transit data for the weights. Our experience shows that these methods often result in underestimated uncertainties of the modeled parameters. To estimate realistic parameter uncertainties we employ two methods. First we rescaled the photometric weights  $\sigma_j$  so that the best-fitting model for each band and run results in a reduced  $\chi^2 = 1$ , which therefore requires the initial values for the photometric uncertainties to be multiplied by the factors  $\chi_{\text{red}}^2 = 1.396$ ,  $\chi_{\text{red}}^2 = 1.058$  and  $\chi_{\text{red}}^2 = 1.179$ , for the UT August 26 and 30 and October 8 2009 runs, respectively.

Second, we take into account the “red noise” in our data by following the “time-averaging” approach that was proposed by Pont et al. (2006) and used in the transit data analysis of various authors including Gillon et al. (2006), Winn et al. (2007, 2008, 2009) and Gibson et al. (2008). The main idea of the method is to compute the standard deviation (scatter) of the unbinned residuals between the observed and calculated fluxes,  $\sigma_1$  and also the standard deviation of the time-averaged residuals,  $\sigma_N$ , where the flux of each  $N$  data points were averaged creating  $M$  bins. In the absence of red noise one would expect

$$\sigma_N = \frac{\sigma_1}{\sqrt{N}} \sqrt{\frac{M}{M-1}}. \quad (5)$$

However, in reality  $\sigma_N$  is larger than  $\sigma_1$  by some factor  $\beta$ , which, as pointed out by Winn et al. (2007), is specific to each parameter of the fitted model. For simplicity we assume that the values of  $\beta$  are the same for all parameters and find its value by averaging  $\beta$  over a range of bins with timescales consistent with the duration of the transit ingress or egress i.e. 10 – 30 min. The resulting values for  $\beta$  are then used to rescale  $\sigma_j$  in the  $\chi^2$  by this value (see Table 4)

To derive transit mid-times ( $T_C$ ) we fixed the orbital period  $P$  to an initial value taken from Sanchis-Ojeda et al. (2011) and fitted the light curves from each run for the best  $T_C$ , planet to star size ratio, inclination and normalized semimajor axis. We then find the best orbital period  $P$  and  $T_C$  using the method discussed in 4.2. Then we take the new values for the  $T_C$  and  $P$  and repeat the fit for the best planet to star size ratio, inclination and normalized semimajor axis. This procedure is iterated until we obtain a consistent solution.

## 4. Results

### 4.1. System parameters

We set the mass and radius of the star equal to  $0.92 \pm 0.06 M_\odot$  and  $0.907_{+0.014}^{-0.013} R_*$ , respectively, and determine the best-fit radius for WASP-4b,  $R_p$  by minimizing the  $\chi^2$  function over the four band-passes and the three runs simultaneously. Furthermore,

**Table 4.** Summary of the residual r.m.s. (observed minus calculated flux) of the unbinned and binned data.

run	band	$\sigma$ [mag]	$\beta$	$\sigma_{\text{sys}}$ [mag]
Aug 26	$g'$	0.0025	1.41	0.0035
Aug 26	$r'$	0.0025	1.38	0.0035
Aug 26	$i'$	0.0028	1.45	0.0041
Aug 26	$z'$	0.0028	1.49	0.0042
Aug 30	$g'$	0.0023	1.19	0.0027
Aug 30	$r'$	0.0017	1.10	0.0019
Aug 30	$i'$	0.0025	1.23	0.0031
Aug 30	$z'$	0.0022	1.29	0.0028
Oct 08	$g'$	0.0018	1.22	0.0022
Oct 08	$r'$	0.0018	1.17	0.0021
Oct 08	$i'$	0.0019	1.29	0.0025
Oct 08	$z'$	0.0020	1.33	0.0027

**Notes.**  $\sigma$  represents the residual scatter over the entire observing time interval on each run;  $\sigma_{\text{sys}}$  is the rescaled value for the photometric weights, reflecting the presence of red noise.

we assume that the inclination and the semimajor axis of the planetary orbit should not depend on the observed pass-band. Therefore, we constrained these parameters to a single universal value. Following this procedure for the radius of the planet we found  $1.413 \pm 0.020 R_{\text{Jup}}$  and the best-fit value for the orbital inclination and semimajor axis  $i = 88.57^\circ \pm 0.45^\circ$  and  $a = 0.02300 \pm 0.00036$  AU, respectively. For comparison of the key parameter,  $R_p$ , Wilson et al. (2008) derived  $1.416_{-0.043}^{+0.068} R_{\text{Jup}}$ , Gillon et al. (2008) derived  $1.304_{-0.042}^{+0.054} R_{\text{Jup}}$ , Winn et al. (2009) derived  $1.365 \pm 0.021 R_{\text{Jup}}$ , Southworth et al. (2009) derived  $1.371_{-0.035}^{+0.032} R_{\text{Jup}}$  and Sanchis-Ojeda et al. (2011) derived  $1.363 \pm 0.020 R_{\text{Jup}}$ . Our value for  $R_p$  is slightly higher than the cited radius in the literature and is dominated by the uncertainty of the stellar radius  $R_*$ . The value for the orbital inclination, from our analysis is in a good agreement with earlier results. For example, Winn et al. (2009) found  $88.56_{+0.98}^{-0.46}$ , Sanchis-Ojeda et al. (2011) found  $88.80_{+0.61}^{-0.43}$ , while Gillon et al. (2009) and Southworth et al. (2009) found  $89.35_{-0.49}^{+0.64}$  and  $88.80^\circ - 90.00^\circ$ , respectively. The results for the fitted parameters of the transit light curve modelling allow us to derive a set of physical properties for the WASP-4 system. Table 3 exhibits a complete list of these quantities.

To complete the light curve analysis we further fit the light curves allowing the linear and the quadratic limb darkening coefficients ( $u_1$  and  $u_2$ ) in each pass-band to be treated as free parameters. We aim to compare the shapes of the transit light curves and the fitted system parameters from this fit and the curves derived using theoretically predicted limb darkening coefficients. In order to minimize the  $\chi^2$ -statistic using all of the 11 parameters, including 8 limb darkening coefficients we again employed the downhill simplex algorithm and the bootstrap method. The new parameter values we find  $R_p = 1.409 \pm 0.020 R_{\text{Jup}}$ ,  $i = 88.75^\circ \pm 0.40^\circ$ ,  $a = 0.02298 \pm 0.00033$  AU result in a slightly smaller value of the  $\chi_{\text{red}}^2$  function (1.001), as the fit is able to remove some trends in the data. However, we report the parameter values derived using the theoretically predicted limb darkening coefficient as final results because the new fit is also more sensitive to systematics in the light curve photometry.

A set of multi-band transit light curves also allows one to search for a dependence of the planetary radius,  $R_p$  as a function of the wavelength. Variations of  $R_p$  in some of the pass-bands could be produced by absorption lines such as water va-

**Table 3.** System parameters of the WASP-4 system derived from the light curve analysis.

Parameter		Value	68.3 % Conf. Limits	Unit	Comment
– <i>Light curve fit</i> –					
Planet-to-star size ratio	$p = R_p/R_*$	0.15655	0.00028	–	1
Orbital inclination	$i$	88.57	0.45	deg	1
Normalized semimajor axis	$a/R_*$	5.455	0.031	–	1
Transit impact parameter	$b = (a/R_*) \cos i$	0.136	0.043	–	1
Reduced chi-square	$\chi_{\text{red}}^2$	1.005	–	–	1
– <i>Planetary parameters</i> –					
Radius	$R_p$	1.413	0.020	$R_{Jup}$	2
Semimajor axis	$a$	0.02300	0.00036	AU	2
Mean density	$\rho_p$	0.582	0.036	$\rho_{Jup}$	2
Surface gravity	$g_p$	15.36	0.91	$\text{m s}^{-2}$	2
Transit duration	$t_D$	2.1696	0.0047	hour	1
Ingress/egress	$t_{\text{ing/egr}}$	0.3014	0.0039	hour	1
– <i>Stellar parameters</i> –					
Mean density	$\rho_*$	1.715	0.029	$\text{g cm}^{-3}$	1
$g'$ Linear limb-darkening coefficient	$u_1$	0.616	0.046	–	1
$g'$ Quadratic limb-darkening coefficient	$u_2$	0.211	0.060	–	1
$r'$ Linear limb-darkening coefficient	$u_1$	0.427	0.044	–	1
$r'$ Quadratic limb-darkening coefficient	$u_2$	0.303	0.064	–	1
$i'$ Linear limb-darkening coefficient	$u_1$	0.292	0.047	–	1
$i'$ Quadratic limb-darkening coefficient	$u_2$	0.304	0.060	–	1
$z'$ Linear limb-darkening coefficient	$u_1$	0.241	0.045	–	1
$z'$ Quadratic limb-darkening coefficient	$u_2$	0.386	0.063	–	1

**Notes.** (1) Based on the analysis of the multi-band light curves presented in this work; (2) Values obtained using (1) and results for the  $M_*$ ,  $R_*$ ,  $T_{\text{eff}}$  and  $M_p$  from Winn et al. (2009) and Sanchis-Ojeda et al. (2011).

**Table 5.** Best-fit radius in each band.

band	$\lambda$ (nm)	Radius $R_{Jup}$
$g'$	455	$1.409 \pm 0.021$
$r'$	627	$1.415 \pm 0.020$
$i'$	763	$1.407 \pm 0.021$
$z'$	893	$1.420 \pm 0.021$

**Notes.** The best-fit radii were derived after fixing the orbital inclination and normalized semimajor axis to their best-fit values from Table 3.

por, methane, etc. in the planetary atmosphere. As a check for this assumption we fitted the data originating from each pass-band individually. Instead of fixing  $R_p/R_*$ ,  $i$  and  $a/R_*$  to a single universal value we set the planet to star radius ratio as a free parameter and keep the remaining quantities as free parameters. Table 5 displays the best-fit radii as a function of the wavelength with no indications of variations within the measured errorbars.

#### 4.2. Deriving the transit ephemeris

One of our primary goals is to measure an accurate value for the transit ephemeris ( $T_0$  and  $P$ ). We include all available light curves from the three runs and fit for the locations of minimum light using the best-fit planetary radius, inclination and semimajor axis from Sect. (4.1.). We minimize the  $\chi^2$  as defined in Sect. (4) over the four-band data of each run by fitting simultaneously for the  $T_C$ . After the best-fit transit mid-times are derived we add them to all reported transit mid-times available at the time of writing in the literature<sup>2</sup> (Table 5). We further fit for the or-

bital period  $P$  and the reference transit epoch  $T_0$  by plotting the transit mid-times as a function of the observed epoch ( $E$ )

$$T_C(E) = T_0 + E \times P. \quad (6)$$

In this linear fit the constant coefficient is the best-fit reference transit epoch ( $T_0$ ) and the slope of the line is the planetary period,  $P$ . We then use the new values for the period and the reference epoch to repeat our fitting procedure for the system parameters until we arrive at a point of convergence. We used the on-line converter developed by Eastman et al. (2010) and transformed the transit mid-times from JD based on UTC to BJD based on the Barycentric Dynamical Time (TDB). We derive a Period =  $1.33823144 \pm 0.00000032$  day and a reference transit time  $T_C = 2454697.798311 \pm 0.000046$  BJD. The result for the best-fit period is consistent with the one from Sanchis-Ojeda et al. (2011), who found  $P = 1.33823187 \pm 0.00000025$  day, and reported a smaller error as they measured the period using all available transit times, including the four additional measurements reported by Southworth et al. (2009).

We further investigated the observed minus calculated ( $O - C$ ) residuals of our data and the reported transit mid-times at the time of writing for any departures from the predicted values estimated using our ephemeris. As it was shown by Holman & Murray (2005) and Agol et al. (2005) a deviation in the  $O - C$  values can potentially reveal the presence of moons or additional planets in the system. We list and plot the  $O - C$  values from our analysis in Table 5 and Figure 3, respectively. An analysis of the  $O - C$  values shows no sign of a TTV signal greater than 20 s, except the two big outliers at epochs 300 and 305. We put upper constraints on the mass of an additional perturbing planet in

<sup>2</sup> Southworth et al. (2009) measured mid-times during four transits of WASP-4b. We exclude these times in our analysis, as they were reported

as unreliable due to technical issues associated with the computer clock at the time of observations (Southworth 2011, private communication)

**Table 6.** Literature transit mid-times of WASP-4 and their residuals in addition to the ephemeris derived in this work.

Epoch	Transit midtime (BJD)	O – C (day)	Reference
0	2453963.1094 <sup>+0.0025</sup>	0.00011	1
300	2454364.5765 <sup>+0.0021</sup> <sub>-0.0033</sub>	-0.00223	1
303	2454368.59341 <sup>+0.00025</sup> <sub>-0.00027</sub>	0.00003	1
305	2454371.26813 <sup>+0.00097</sup> <sub>-0.00087</sub>	-0.00171	1
324	2454396.69623 <sup>+0.00015</sup> <sub>-0.00026</sub>	-0.00001	1
549	2454697.798228 <sup>+0.000055</sup> <sub>-0.000055</sub>	-0.00008	2
587	2454748.651228 <sup>+0.000072</sup> <sub>-0.000072</sub>	0.00012	2
809	2455045.738643 <sup>+0.000054</sup> <sub>-0.000054</sub>	0.00016	3
812	2455049.753274 <sup>+0.000054</sup> <sub>-0.000066</sub>	0.00010	3
815	2455053.767816 <sup>+0.000053</sup> <sub>-0.000053</sub>	-0.00006	3
827	2455069.826637 <sup>+0.000086</sup> <sub>-0.000086</sub>	-0.00001	4
830	2455073.841103 <sup>+0.000070</sup> <sub>-0.000061</sub>	-0.00024	4
850	2455100.605928 <sup>+0.000061</sup> <sub>-0.000061</sub>	-0.00005	3
859	2455112.650002 <sup>+0.000074</sup> <sub>-0.000074</sub>	-0.00005	4

**Notes.** (1) Gillon et al. (2009); (2) Winn et al. (2009); (3) Sanchis-Ojeda et al. (2011); (4) This work; The epoch of the first observed transit of WASP-4b was taken as equal to zero.

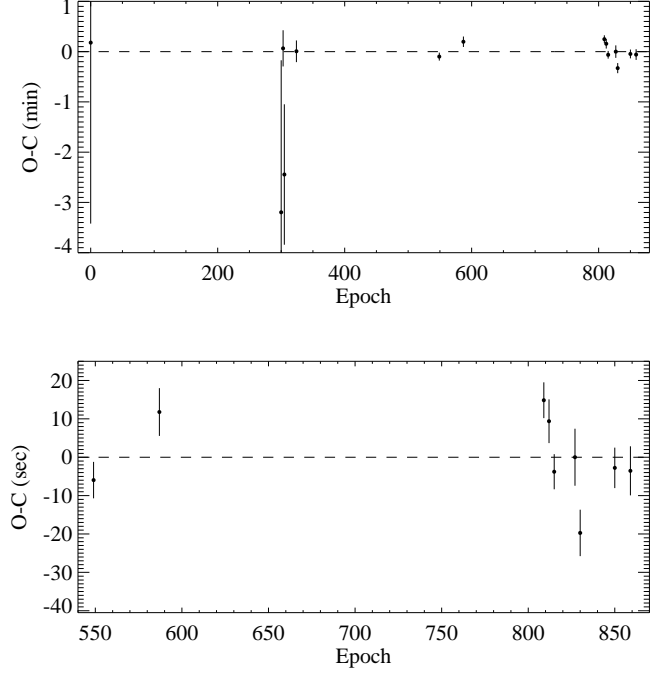
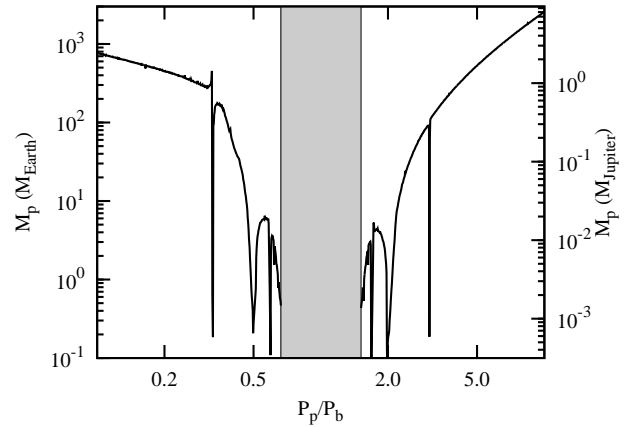
the system as a function of its orbital parameters. We simplified the three-body problem by assuming that the system is coplanar and initial orbits of both planets are circular. The orbital period of the perturber was varied in a range between 0.1 and 10 orbital periods of WASP-4b. We generated 1000 synthetic  $O - C$  diagrams based on calculations done with the MERCURY package (Chambers 1999). We applied the Bulirsch–Stoer algorithm to integrate the equations of motion. Calculations covered 1150 days, i.e. 860 periods of the transiting planet, that are covered by observations. The results of simulations are presented in Fig. 4. Our analysis allows us to exclude additional Earth-mass planets close to low-order period commensurabilities with WASP-4b.

For the case of a transiting planet with a semi-major axis  $a_1$  and period  $P_1$  and a perturbing planet with semi-major axis  $a_2$  on an outer orbit (i.e.  $a_2 \geq a_1$ ), period  $P_2$  and mass  $M_2$  Holman & Murray 2005 derived the approximate formula

$$\Delta t \simeq \frac{45\pi}{16} \left( \frac{M_2}{M_*} \right) P_1 \alpha_e^3 (1 - \sqrt{2}\alpha_e^{3/2})^{-2} \quad (7)$$

$$\alpha_e = \frac{a_1}{a_2(1 - e_2)} \quad (8)$$

for the magnitude of the variation (in seconds) of the time interval ( $\Delta t$ ) between successive transits. One could imagine an exterior perturbing planet on a circular coplanar orbit twice as far as WASP-4b (period  $P \approx 3.75$  day not in mean motion resonance with the transiting planet). If such an imaginary planet had a mass of  $0.1M_{\text{Jup}}$ , it would have induced  $\sim 5$  sec variations in the predicted transit mid-times of WASP-4b. Furthermore, the perturber could cause radial velocity variations of the parent star  $\sim 13.78$  m/s, which is below the radial velocity r.m.s. of the WASP-4 residual equal to 15.16 m/s, presented in the analysis of Triaud et al. (2010). Although, a few outliers are visible in the  $O - C$  diagram we consider the prediction of such an imaginary planet in the WASP-4 system as immature, because the weights of the  $O - C$  points might still require an additional term to account for systematics of unknown origin.

**Fig. 3.** The transit timing residuals for WASP-4b along with the one sigma errorbars. Top panel: The observed transit mid-times based on this work and others in the literature were subtracted from the calculated times produced by our ephemeris. Lower panel: A closer view of the available transit mid-times from 2009 and 2010.**Fig. 4.** The upper-mass limit of a hypothetical additional planet that could perturb the orbital motion of WASP-4b as a function of ratio of orbital periods of transiting planet,  $P_b$ , and the perturber,  $P_p$ . Orbits located in a grey area were found to be unstable.

## 5. Concluding remarks

We have used the GROND multi-channel instrument to obtain four-band simultaneous light curves of the WASP-4 system during three transits (a total of 12 light curves) with the aim to refine the planet and star parameters and to search for transit timing variations. We derived the final values for the planetary radius  $R_p$  and the orbital inclination  $i$  by fixing the stellar radius  $R_*$  and mass  $M_*$  to the independently derived values of Winn et al. (2009) and Sanchis-Ojeda et al. (2011). We include the

time-correlated “red-noise” in the photometric uncertainties using the “time-averaging” methodology and by rescaling the weights to produce value for the  $\chi^2_{\text{red}}$  equal to unity. We further perform the light curves analysis by minimizing the  $\chi^2$  function over all pass bands and runs simultaneously via two approaches. First we modeled the data using theoretically predicted limb-darkening coefficients for the quadratic law. Second, we fit the light curves for the limb-darkening. Both methods result in consistent system parameters within  $< 1\%$ . The second method produced limb darkening parameters compatible with the theoretical predictions within the one-sigma errorbars of the fitted parameters.

We added three new transit mid-times for WASP-4b, derived a new ephemeris and investigated the  $O - C$  diagram for outlier points. We have not found compelling evidences for outliers that could be produced by the presence of a second planet in the system. We did not detect any short-lived photometric anomalies such as occultations of starspots by the planet, which were detected by Sanchis-Ojeda et al. (2011). At the transit r.m.s. level of our light curves ( $\sim 2.2$  mmag) it would be challenging to detect similar anomalies. However we note that due to the brightness of the parent star, the short planetary orbital period and the significant transit depth, the WASP-4 system is well suited for follow-up observations.

*Acknowledgements.* Part of the funding for GROND (both hardware as well as personnel) was generously granted from the Leibniz-Prize to Prof. G. Hasinger (DFG grant HA 1850/28-1). N.N. acknowledges the Klaus Tschira Stiftung (KTS) and the Heidelberg Graduate School of Fundamental Physics (HGSFP) for the financial support of his PhD research. GM acknowledges the financial support from the Polish Ministry of Science and Higher Education through the Iuventus Plus grant IP2010 023070. The authors would like to acknowledge Luigi Mancini, John Southworth and the anonymous referee by their useful comments and suggestions.

## References

- Agol, E., Steffen, J., Sari, R., & Clarkson, W. 2005, MNRAS, 359, 567  
 Beerer, I.M., Knutson, H.A., Burrows, A., et al. 2011, ApJ, 727, 23  
 Cáceres, C., Ivanov, V.D., Minniti, D., Burrows, A., et al. 2011, A&A, 530, 5  
 Chambers, J.E. 1999, MNRAS, 304, 793  
 Charbonneau, D., Brown, T. M., Latham, D. W., & Mayor, M. 2000, ApJ, 529, L45  
 Claret, A. 2004, A&A, 428, 1001  
 Eastman, J., Siverd, R., Gaudi, B.S., 2010, PASP, 122, 935  
 Gibson, N.P., Pollacco, D., Simpson, E.K., et al. 2008, A&A, 492, 603  
 Gillon, M., Pont, F., Moutou, C., et al. 2006, A&A, 459, 249  
 Gillon, M., Smalley, B., Hebb, L., et al. 2009, A&A, 496, 259  
 Greiner, J., Bornemann, W., Clemens, C., et al. 2008, PASP, 120, 405  
 Grillmair, C.J., Charbonneau, D., Burrows, A., et al. 2007, ApJ, 658, 115  
 Henry, G. W., Marcy, G. W., Butler, R. P., & Vogt, S. S. 2000, ApJ, 529, 41  
 Holman, M. J., & Murray, N. W. 2005, Science, 307, 1288  
 Holman, M. J., Fabrycky, D.C., Ragozzine, D., et al. 2010, Science, 330, 6000  
 Jha, S., Charbonneau, D., Garnavich, P.M., et al. 2000, ApJ, 540, 45J  
 Johnson, J.A., Winn, J.N., Bakos, G. Á., et al. 2011, ApJ, 735, 24  
 Knutson, H.A., Charbonneau, D., Noyes, R.W., Brown, T.M., & Gilliland, R.L. 2007, ApJ, 655, 564  
 Lissauer, J.J., Fabrycky, D.C., Ford, E.B., et al., 2011, Nature, 470, 53  
 Mandel, K. & Agol, E. 2002, ApJ, 580L, 171  
 Mazeh, T., Naef, D. and Torres, G. et al. 2000, ApJ, 532, L55  
 Miralda-Escudé, J., 2002, ApJ, 564, 1019  
 Pollacco, D.L., Skillen, I., Collier Cameron, A., et al. 2006, PASP, 118, 1407  
 Pont, F., Zucker, S., & Queloz, D. 2006, MNRAS, 373, 231  
 Press, W. H., Teukolsky, S. A., Vetterling, W. T., & Flannery, B. P. 1992, Numerical recipes in C. The art of scientific computing, ed. T.S.A.V.W.T.F.B.P. Press, W. H.  
 Queloz, D., Eggenberger, A., Mayor, M., et al. 2000, A&A, 359, 13  
 Richardson, L.J., Deming, D., Horning, K., Seager, S., Harrington, J., 2007, Nature, 445, 892  
 Sanchis-Ojeda, R., Winn, J.N., Holman, M.J., Carter, J.A., Osip, D.J., Fuentes, C.I., 2011, ApJ, 733, 127  
 Southworth, J., Hinse, T.C., Burgdorf, M.J., et al. 2009, MNRAS, 399, 287

- Triard, A.H.M.J., Collier Cameron, A., Queloz, D., et al. 2010, A&A, 524, 25  
 Winn, J. N. Holman, M.J. and Henry, G.W., et al. 2007, AJ, 133, 1828  
 Winn, J.N., Holman, M.J., Torres, G., et al. 2008, ApJ, 683, 1076  
 Winn, J.N., Holman, M.J., Carter, J.A., et al. 2009, AJ, 137, 3826  
 Winn, J.N., Howard, A.W., Johnson, J.A., et al. 2011, AJ, 141, 63  
 Wilson, D.M., Gillon, M., Hellier, C., et al. 2008, ApJ, 675, L113